

Single Molecule Tracking Studies of Flow-Aligned Mesoporous Silica Monoliths: Aging-Time Dependence of Pore Order

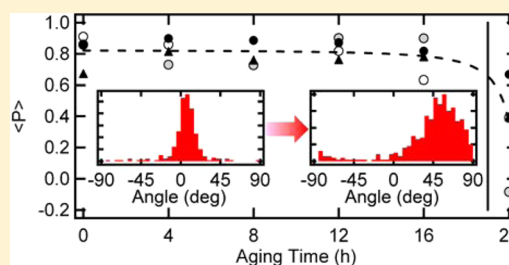
Seok Chan Park, Takashi Ito,* and Daniel A. Higgins*

Department of Chemistry, Kansas State University, Manhattan, Kansas 66506-0401, United States

S Supporting Information

ABSTRACT: Single molecule tracking (SMT) methods are employed to characterize the in-plane alignment and order of cylindrical mesopores in flow-aligned surfactant-templated silica monoliths prepared within glass microfluidic channels. The majority of dye molecules observed in wide-field fluorescence videos of these samples exhibit one-dimensional (1D) diffusive motions. Orthogonal regression analysis of these motions provides a measure of the mesopore orientation distribution function, which in turn is used to quantify the mesopore order via a two-dimensional orientational order parameter, $\langle P \rangle$. Mesopore organization is explored as a function of aging time between sol preparation and filling of the microfluidic channels.

Channels filled well before gelation of the sol are shown to incorporate large monodomains having average pore alignment within a few degrees of the flow direction. These monodomains extend over several millimeters and yield aging-time-independent $\langle P \rangle$ values larger than ~ 0.80 . In contrast, channels filled near the time of sol gelation yield monoliths with misaligned pores that are also more disordered, having $\langle P \rangle \approx 0.35$. The SMT results are compared to those from small-angle X-ray scattering anisotropy experiments; these data are consistent across the range of samples investigated. A model describing the aging-time dependence of sol organization is presented. These studies demonstrate that well-aligned mesoporous silica monoliths can be obtained by simple flow alignment procedures but that short sol aging times are required in order to achieve optimum pore organization.



■ INTRODUCTION

Surfactant-templated mesoporous silica materials find a range of possible applications in catalysis, chemical sensing, separations, and molecular sieving.^{1–4} Such materials are prepared by the hydrolysis and condensation of alkoxysilane precursors in the presence of structure-directing agents such as surfactant micelles. Depending on the synthetic conditions employed, materials incorporating spherical, planar, or cylindrical surfactant structures organized in cubic, lamellar, or hexagonal configurations can be produced.^{3,5} Mesoporous materials derived from hexagonally arranged cylindrical micelles are most common and are the subject of this report. Polymerization of the inorganic silica matrix around these micelles produces rigid glass materials incorporating hexagonally organized cylindrical mesopores.

Pore alignment is largely uncontrolled in most such syntheses, resulting in “polycrystalline” materials incorporating randomly aligned domains of otherwise well-organized pores. However, optimum performance in many of their applications (i.e., membranes for chemical separations) requires the fabrication of pores aligned along a particular predefined direction. As a result, several research groups have developed methods for preparing aligned mesoporous materials.^{4,5} For example, Chmelka and co-workers demonstrated that exposure of a surfactant-templated sol to a strong magnetic field⁷ produces aligned mesopores upon gelation of the sol. Walcarius and co-workers have described electrochemically assisted self-assembly methods for synthesizing silica films incorporating

one-dimensional (1D) mesopores oriented perpendicular to an underlying electrode surface.^{8,9} Interactions with substrate surface structures have also been employed to produce aligned mesopores. Representative methods include deposition of surfactant-templated sols on rubbed polyimide films,¹⁰ single-crystal substrates,¹¹ and lithographically prepared surface nanostructures.¹² Some of the simplest methods for obtaining aligned mesoporous materials, however, involve the injection of surfactant-containing sols into confining structures,⁴ such as the pores of anodic alumina membranes,^{13,14} glass capillaries,¹⁵ or microfluidic channels.^{16,17} In capillaries and microfluidic channels, micelle (and pore) alignment often results from shearing of the surfactant mesophase.¹⁸

The physical properties of mesoporous materials are commonly assessed by electron microscopy (EM),^{1,8–11,13–15} small-angle X-ray scattering (SAXS),^{1,7,9–11} and NMR spectroscopy.⁷ EM provides high-resolution visual evidence of local mesopore structure and orientation but requires significant effort to detect long-range organization. It also involves placing the sample under vacuum and hence the removal of any solvent. Likewise, SAXS affords detailed physical insights into mesopore morphology and alignment, but the data obtained largely reflect average materials properties. Unfortunately,

Special Issue: Paul F. Barbara Memorial Issue

Received: April 13, 2012

Revised: July 10, 2012

Published: July 31, 2012

neither EM nor SAXS provides direct data on the mass-transport characteristics of the materials. NMR methods provide an important route for obtaining such dynamical information (i.e., rate and anisotropy of probe diffusion) along with data on long-range mesopore alignment. However, like SAXS, the information obtained is averaged over relatively large sample regions.

It has recently been demonstrated by the Bräuchle group^{17,19–21} and others^{6,22} that single molecule tracking (SMT) methods²³ can be used to directly observe the motions of individual fluorescent molecules diffusing within discrete nanometer-sized cylindrical channels of surfactant-templated mesoporous silica. Identical experiments on similarly structured materials are now also being reported.^{24,25} SMT methods represent important tools for the investigation of mesoporous systems because they allow for (i) the materials structure to be visualized,^{6,17} (ii) the occurrence of 1D mass transport to be directly observed, (iii) molecular mobility within *individual* pores to be quantified, and (iv) the alignment and organization of single mesopores to be assessed. While such methods have been used previously to assess materials organization qualitatively, recent work from our lab has shown that quantitative information on mesopore orientational alignment and ordering can be obtained via orthogonal regression analysis of single molecule trajectory data.⁶ We have used these methods to characterize the mesopore alignment and order in spin-coated silica films,⁶ the alignment of cylindrical surfactant micelles in lyotropic liquid-crystal mesophases,²⁴ and the alignment of cylindrical domains in block copolymer films.²⁶ Importantly, the ability to observe molecular motions at the single-event level also enables the investigation of materials heterogeneity. For example, in our studies of spin-coated silica films, SMT data revealed the presence of distinct domains having different average pore orientations but similar levels of pore order.⁶ Such information would be lost in SAXS measurements when the domain size is smaller than the incident beam size.

In this work, macroscopically aligned mesoporous silica monoliths were prepared by flow alignment of surfactant-templated silica sols in etched-glass microfluidic channels. Cetyltrimethylammonium bromide (CTAB) was employed as the surfactant and was present at sufficient concentration to form the hexagonal mesophase in the precursor sol. The mesopore alignment and organization in each sample were assessed by both SMT and SAXS. The primary goal of these investigations was to characterize the mesopore organization as a function of sol aging time (i.e., the time between sol preparation and injection into the microfluidic channel). A fluorescent perylenediimide dye, *N,N'*-bis(octyloxypropyl)-perylene-3,4,9,10-tetracarboxylic diimide (OPDI),⁶ whose structure is shown in Figure S1 in the Supporting Information, was employed as the probe molecule. Wide-field fluorescence videos depicting OPDI motions at the single-molecule/single-pore level revealed a predominance of 1D diffusion. Orthogonal regression analysis of the trajectory data provided quantitative information on the in-plane orientation of individual pores. The degree to which the pores were aligned along the flow direction was assessed in each sample, as was the mesopore order, which was quantified by calculation of a two-dimensional (2D) order parameter from the individual trajectory angles. The results obtained were compared to those from SAXS experiments. Taken together, the results showed that materials prepared well before gelation of the sol incorporate large monodomains that

extend over millimeter length scales. The mesopores within these monodomains were closely aligned with the flow direction and were well-ordered. In contrast, materials prepared close to the time of sol gelation were often misaligned and always more disordered.

■ EXPERIMENTAL SECTION

Sample Preparation. Silica sols were prepared from tetramethoxysilane (TMOS) (99%, Aldrich), acidified water (HPLC grade, pH ~2), and CTAB (Aldrich). The first step in the procedure was to mix 0.250 g of TMOS with 1 mL of acidified water, with stirring. The methanol generated by the hydrolysis of TMOS was then removed under vacuum.¹⁵ CTAB (0.6 g) was subsequently dissolved in the sol by vigorous stirring and by repeated inversion while centrifuging. For SMT experiments, all of the samples were doped to nanomolar concentrations with OPDI by addition of 10 μ L of 200 nM ethanolic dye solution to the sol, yielding a final dye concentration of ~2 nM. Sols prepared in this manner fall within the hexagonal region of the ternary CTAB/water/ethanol phase diagram.²⁷ The sols were subsequently aged at 35 °C in the dark for a period of 0–20 h. Finally, they were injected into microfluidic channels and capillaries for characterization by SMT and SAXS, respectively. The gelation time for the sol was determined by checking the sol fluidity at 15 min intervals after 17 h. The sol fluidity was assessed by inverting the vial and observing whether the sol flowed over the course of 10 min. The sols were concluded to gel 19 ± 1 h after preparation.

Microfluidic Channel Design and Fabrication. Microfluidic chips were designed to incorporate rectangular channels of 70 μ m depth, 15 mm length, and 2 mm width (Figure 1a). The channels were etched into microscope slides (FisherFinest Premium) using a buffered NH_4F oxide etchant (Transene Co.).²⁸ The channel dimensions were defined using patterned commercial electrical tape contacted to the slide glass. After etching, the tape was removed and the slides were rinsed using 18 M Ω cm water. Channel depths were measured using a surface profiler (Ambios Technology). Once the channel was etched to the desired depth, 1 mm diameter inlet and outlet holes were mechanically drilled at its ends.

Each etched slide was then bonded to a microscope coverslip (FisherFinest Premium) to form a microfluidic cell.²⁸ Before assembly of the cell, the slide and coverslip were thoroughly cleaned using a multistep process. First, the etched slide and coverslip were submerged in warm soap water, sonicated for 10 min, and rinsed with 18 M Ω cm water. They were subsequently sonicated in a warm 10 wt % NaOH solution and again rinsed. Next, they were immersed in 5 vol % H_2SO_4 . Immediately after a final rinse in 18 M Ω cm water, the slide and coverslip were pressed together using binder clips. The assembled chips were then placed in an oven at 45 °C for 30 min to evaporate remaining water and prebond the two pieces of glass. Finally, the cells were transferred to a furnace and permanently bonded by heating at 350 °C for 12 h.

Flow Alignment of Sols. Silica sols were aged for 0, 4, 8, 12, 16, and 20 h prior to loading into the microfluidic channels and capillaries. Sols aged beyond 20 h could not be infused into the microfluidic channels. For filling of the microfluidic channels, the sol was first drawn into a glass capillary using a syringe pump. The capillary was then inserted into the channel inlet, and the syringe pump was reversed to introduce the sol into the channel. Sol was pumped into the channel at a flow

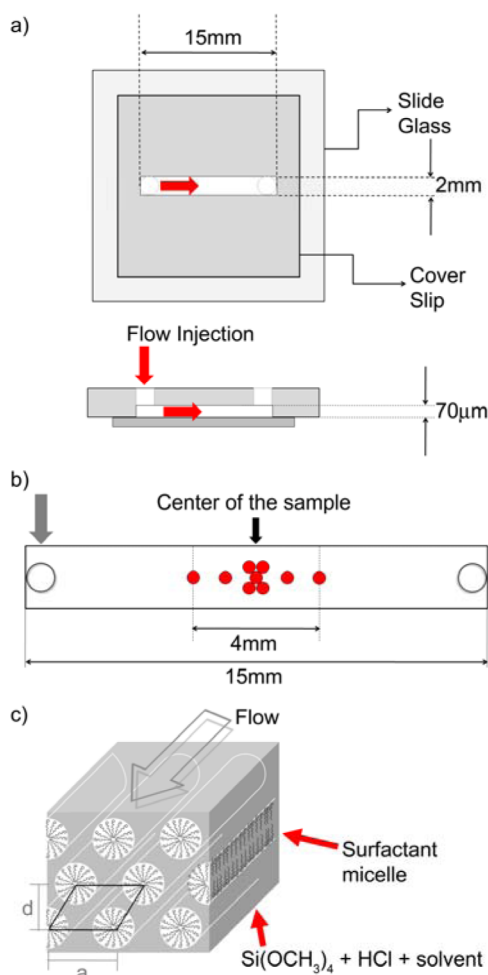


Figure 1. (a) Etched-glass microfluidic cell employed to obtain flow-aligned mesoporous silica monoliths for SMT experiments. The cell consists of an etched microscope slide incorporating a rectangular channel 15 mm long, 2 mm wide, and 70 μm deep with inlet and outlet holes drilled through the glass at the channel ends. A microscope cover glass is bonded to the slide to enclose the channel and allow for imaging with a high-NA objective. (b) Locations at which SMT measurements were made within each monolith (red circles). (c) Model of flow-aligned, hexagonally arranged cylindrical surfactant micelles in mesoporous silica.

velocity of ~ 12 mm/min. Once the channel was filled, the inlet and outlet holes were sealed using two-part five minute epoxy. The microfluidic chips were then stored for one additional day at 35 $^{\circ}\text{C}$ in the dark to ensure that the sol had gelled in each case.

Single Molecule Tracking. All of the SMT experiments were conducted on a wide-field fluorescence microscope operated in the through-objective total internal reflection fluorescence (TIRF) mode.²³ The optical microscope employed has been described previously.^{6,24} For excitation of the dye, 488 nm light from a blue diode laser was employed. The incident laser power was maintained at 4 mW in all experiments. In most cases, the incident light was linearly polarized parallel to the microfluidic channel axis. An electron-multiplying CCD camera (Andor iXon DU-897) was used to detect sample emission at all polarizations.

TIRF videos were collected from nine different locations in each monolith (Figure 1b). Five of these were collected at evenly spaced 1 mm intervals along the centerline of the

monolith. Four additional measurements were made at points displaced vertically and horizontally from the monolith center by a distance of 300 μm . Videos were acquired as 1000-frame sequences with a cycle time of 0.042 s per frame using an electron-multiplying gain of 30 and a 10 MHz readout rate. Camera pixels were binned in a 2×2 configuration, giving a calibrated image pixel size of 125 nm. Unbiased excitation and detection of the molecules was verified by exciting the sample with linearly polarized light having orthogonal polarizations (perpendicular and parallel to the channel axis), with circularly polarized light, and with the microfluidic channel oriented in orthogonal directions on the microscope stage (see Figure S2 and Table S1 in the Supporting Information). The number of molecules detected was independent of the sample orientation on the microscope stage, and the level of sample order was invariant with respect to incident polarization and sample orientation.

2D SAXS Measurements. The 2D SAXS measurements were performed at the Characterization Facility at the University of Minnesota (Minneapolis, MN) using a SAXS instrument incorporating a Rigaku 12 kW Cu rotating-anode source ($\lambda = 1.54$ \AA) and a multiwire area detector. The sample-to-detector distance was 59.5 cm. As in the SMT experiments, sols aged for 0, 4, 8, 12, 16, and 20 h were prepared and characterized. In this case, the sols were drawn into 1 mm diameter thin-walled capillaries (10 μm wall thickness; Charles Supper Co.). The capillaries were then flame-sealed. Several replicate SAXS patterns were acquired for each sample with an exposure time of 300 s.

RESULTS

2D SAXS Measurements. The SAXS pattern obtained from a representative flow-aligned mesoporous silica monolith is shown in the Figure 2a inset. The capillary from which these data were acquired was oriented along the vertical direction in the figure. The bright regions on either side of the X-ray beam (center) demonstrate that the scattering was strongest in the plane perpendicular to the capillary axis. The scattering intensity as a function of 2θ is also plotted in Figure 2a. These data are consistent with the presence of hexagonally ordered cylindrical mesopores.²⁹ The characteristic (100) peak appeared at $2\theta \approx 1.67^{\circ}$, which corresponds to a d spacing of 52.8 ± 0.3 \AA (from multiple measurements). The d spacing in this case is significantly larger than previously reported for dry^{6,29} and/or calcined mesoporous silica.^{1,29} This discrepancy is attributable to swelling of the surfactant micelles in the wet gels being investigated. Importantly, the d spacing was found to be independent of sol aging time, as shown in Figure 2b.

Information on the mesopore alignment and order was obtained by plotting the SAXS data as a function of azimuthal angle, χ , as shown in Figure 2c. The observation of strong scattering in the plane perpendicular to the capillary axis demonstrates that the mesopores were aligned parallel to the flow direction on average, as depicted in Figure 1c. Qualitatively, the sharpness of the scattering peak in χ indicates that the mesopores are relatively well-ordered for short sol aging times (see Figure 2c, 4 h data). The SAXS anisotropy data obtained for longer aging times showed a trend in the mesopore order that is consistent with the results of the SMT experiments (see below). In particular, the incorporation of misaligned mesophases and a dramatic decrease in materials order was observed for capillaries filled near the time of sol gelation (see Figure 2c, 20 h data).

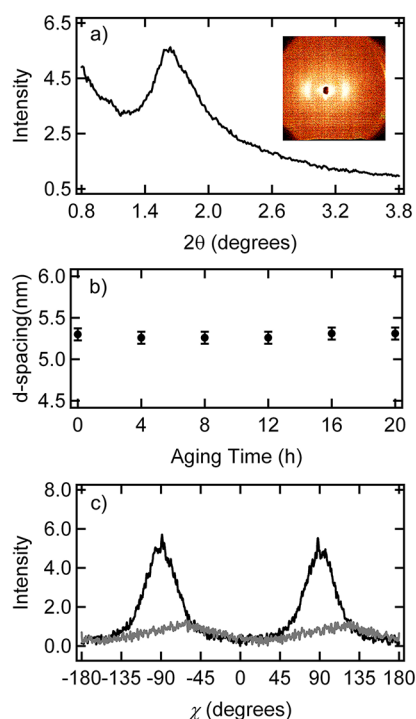


Figure 2. (a) X-ray scattering intensity as a function of scattering angle (2θ) derived from the 2D SAXS pattern shown in the inset. The data were obtained from a flow-aligned mesoporous silica monolith prepared within a cylindrical glass capillary from a sol aged for 4 h. The capillary was oriented along the vertical direction on the scattering pattern (see the inset). (b) Characteristic d spacing for hexagonally arranged cylindrical mesopores in the silica monoliths as a function of sol aging time. The data demonstrate that mesopore spacing was independent of the sol aging time. Error bars depict the 95% confidence intervals about the mean. (c) Scattering intensity as a function of azimuthal angle, χ , from sols aged for 4 h (black) and 20 h (gray). Here $\chi = 0^\circ$ corresponds to the long axis of the capillary.

Single Molecule Tracking Studies. The diffusion of single molecules in the mesoporous silica monoliths was investigated by recording wide-field TIRF-mode videos.²³ TIRF imaging selectively probes molecules near the gel–glass interface and facilitates SMT by limiting the background fluorescence from dye molecules at different depths in the monolith. The depth probed was limited to ~ 200 nm (i.e., the $1/e^2$ distance) by the decay of the evanescent fields from the gel–glass interface.

A representative wide-field image of a flow-aligned silica monolith (prepared from a 4 h aged sol) is shown in Figure 3a. This image was generated by combining all 1000 frames from a single video using the Z-project routine in the ImageJ software package; it depicts the maximum intensity observed at each pixel in the video. The original video is provided in the Supporting Information. Clearly apparent in the image are a large number of horizontal streaks. These streaks demonstrate the predominance of 1D diffusion by the individual OPDI molecules. The observation of 1D molecular motion is consistent with the presence of open (albeit surfactant-filled) cylindrical mesopores in the silica monoliths. The SMT data also demonstrate that the mesopores were aligned predominantly along the flow direction (Figure 1c). Along with molecules exhibiting 1D diffusion, immobile molecules were also found in the videos (e.g., round spots shown in Figure 3a). Mobile and immobile molecules were distinguished by

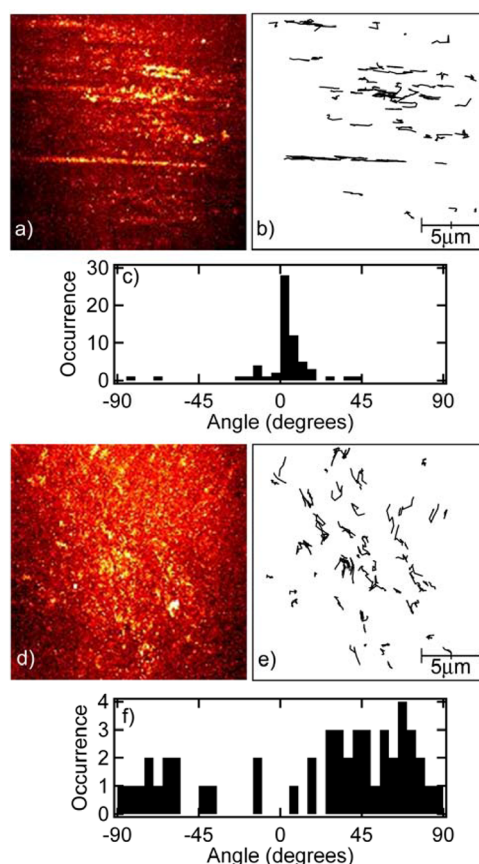


Figure 3. (a) Representative wide-field fluorescence image of a flow-aligned monolith prepared from a sol aged for 4 h. This image was obtained using the Z-project routine in ImageJ and shows the maximum intensity for each pixel observed in the associated video. (b) Single-molecule trajectories obtained from the same video. (c) Histogram showing the trajectory angles relative to the flow axis (0°) in the microfluidic channel. (d–f) Similar data obtained from a flow-aligned monolith prepared from a sol aged for 20 h.

comparing the single-molecule localization precision⁶ (calculated using eq 7 in ref 6; 63 nm on average) with the frame-to-frame mean-square displacement (MSD) for each molecule. Those spots exhibiting MSD values greater than the localization precision at better than 90% confidence were concluded to be mobile. The observation of immobile molecules is ascribed to adsorption of some at the gel–glass interface, while others may be trapped within the silica matrix or in short (i.e., closed) silica mesopores. Such fixed molecules provide no information on materials order and were excluded from further analysis, as discussed below.

For detailed analysis of the single-molecule motions, automated software routines available as an ImageJ plugin³⁰ (modified in house) were employed. Trajectories depicting the motions of the individual molecules within each video were obtained. Only those trajectories >6 frames in length were selected for further analysis. Relatively short trajectories were obtained in the present case because single-molecule diffusion was relatively fast (see below), making it difficult to link the fluorescent spots observed in the video frames into longer trajectories. The trajectory length may also have been limited by blinking of the molecules (i.e., fluorescence intermittency). Trajectories were terminated when the molecule being tracked disappeared for one or more frames. Figure 3b depicts the

trajectories obtained from the video used to generate the image in Figure 3a. They again reflect the predominance of 1D molecular motion.

The single-molecule trajectories incorporate quantitative data on molecular position as a function of time. As we have demonstrated in previous SMT studies,⁶ these data can be fit to a line using orthogonal regression methods³¹ to determine quantitatively the in-plane orientation of each 1D trajectory. This analysis also provides additional statistical data such as the error in the trajectory orientation.⁶ The trajectory angles were used to construct histograms showing the distribution of trajectory orientations. Importantly, as the trajectories depict molecular motions within discrete silica mesopores, they also provide a measure of the pore alignment. Figure 3c presents the distribution of trajectory angles for the data shown in Figure 3b. The histogram is sharply peaked near 0°, corresponding to the approximate direction ($\pm 5^\circ$) of sol flow during filling of the microfluidic channel. While the position of the peak indicates that average pore alignment was along the expected direction, the narrow distribution observed also suggests a high degree of orientational order.

As the main purpose of this work was to explore the dependence of the pore organization on the sol aging time, similar SMT data were collected from a series of samples prepared from sols aged for up to 20 h. A clear trend toward misaligned and disordered mesopores was observed near the time of gelation (~ 19 h; see below). Monoliths prepared from sols aged for 20 h were found to be the most disordered. Figure 3d depicts the representative image obtained from one such sample. The associated video is provided in the Supporting Information. The trajectory data and the trajectory angle histogram obtained from this video are shown in Figure 3e,f. As shown by these data, monoliths prepared from sols aged for 20 h exhibited fewer 1D trajectories. Furthermore, the trajectories recorded from these samples were more randomly aligned and in some cases were even aligned perpendicular to the sol flow direction. It must be noted that some of the trajectories in these samples appeared to depict 2D molecular motion. While the “orientations” of such trajectories were strictly undefined, their fitted values were still included in the pore orientation histograms and subsequent analysis to reflect most properly the true level of mesopore order in these materials.²⁴

Wide-field videos and trajectory data were acquired for three replicate sample series prepared from sols aged for 0, 4, 8, 12, 16, and 20 h (i.e., a total of 18 samples). Data were collected at the nine different locations in each sample defined in Figure 1b. Representative histograms depicting the trajectory orientations for one sample series are shown in Figure 4. These histograms are compilations of trajectory angle data from all nine locations in each sample. Qualitatively, the distributions show that for short aging times, the mesopores were well-aligned (on average) along the expected direction. These data appear to depict a small systematic bias to positive angles. As noted above, samples could only be aligned on the microscope to $\pm 5^\circ$. Single data series such as the one shown in Figure 4 may also exhibit some bias within this range. However, data compiled from measurements on several different samples over several days showed no such bias (see Table 1). The distribution widths reflect a relatively high level of mesopore orientational order that did not vary dramatically with sol aging up to about the time of gelation. The mesopores became misaligned and markedly more disordered in monoliths prepared from sols aged to near the gelation time, as

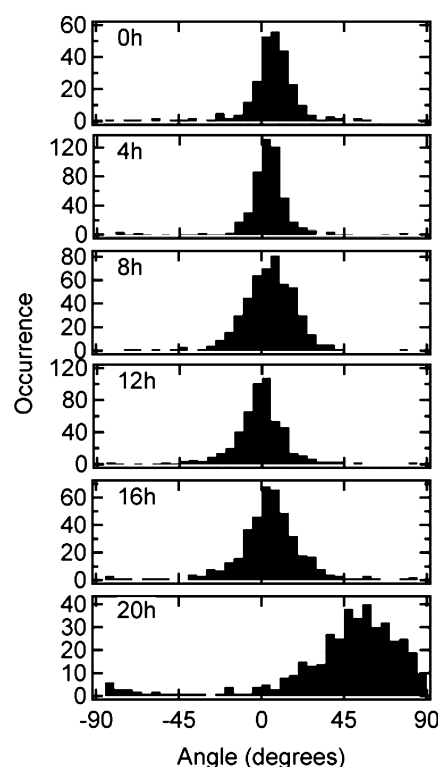


Figure 4. Histograms depicting the trajectory angles compiled from all nine images collected from each sample in a single, representative set of flow-aligned silica samples as a function of sol aging time. The data demonstrate that the mesopores were well-aligned along the flow direction (0°) over distances of several millimeters for materials prepared prior to gelation of the sol at ~ 19 h. Near the gelation time, markedly more disordered and misaligned materials were obtained (see the 20 h data).

demonstrated by the sample aged for 20 h (Figure 4). As noted in the Experimental Section, gelation of these sols occurred at ~ 19 h. The bias to positive angles in this case fell far outside that expected from alignment error on the microscope. Evidence of misaligned mesopores was also observed by SAXS (Figure 2c, 20 h data) in similarly prepared samples.

In our earlier studies of spin-coated mesoporous silica films, it was found from excitation-polarization-dependent imaging that OPDI molecules diffuse within the silica pores in a strongly aligned state,⁶ with their long axes oriented parallel to the pore axis. Such strong orientation of the dye clearly results from its steric confinement within the silica mesopores. In the present samples, the images obtained were largely independent of the excitation polarization (see Figure S2 and Table S1 in the Supporting Information), demonstrating that the alignment measurements were not biased by polarization-selective detection of oriented molecules within pores aligned along the expected direction. These results are also consistent with “rapid” tumbling of the dye within the pores on time scales shorter than the video frame time. The pores in the present samples are concluded to be larger than those in the spin-coated films, as also suggested by the larger d spacing determined from the SAXS data.

Finally, the SMT data also provide the means to assess the mobility of OPDI within the silica mesopores as a function of sol aging time. The apparent diffusion coefficients, D , for individual mobile molecules were determined from their MSD

values over short time scales using the relation $\text{MSD} = 2Dt$ (see Figure S3 in the Supporting Information for representative examples).³² As shown previously, these measurements are somewhat biased to smaller values for short trajectories.²⁴ Figure 5a depicts a histogram of the D values obtained from a

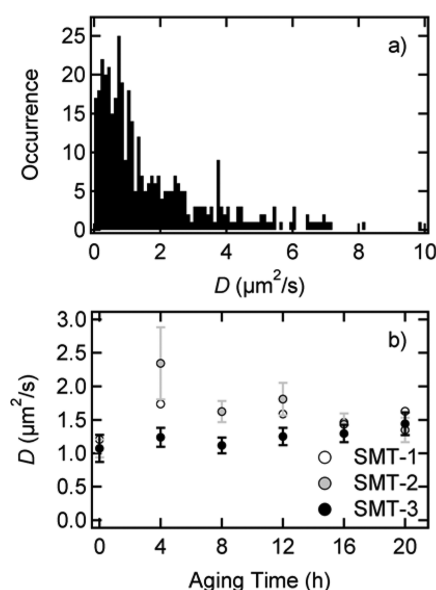


Figure 5. (a) Representative histogram showing diffusion coefficients, D , determined from a single flow-aligned mesoporous silica sample prepared from a sol aged for 4 h. The diffusion coefficients were determined from the MSDs exhibited by individual molecules at short time delays (i.e., five frames). (b) Mean diffusion coefficients obtained as a function of sol aging time for three replicate sample series. No apparent trend is observed in these data, suggesting that the viscosity within the surfactant-containing mesopores is invariant over the range of samples investigated. Error bars depict the 95% confidence interval about the mean in each case.

sample aged for 4 h, from which a mean D value of $1.74 \mu\text{m}^2/\text{s}$ was obtained. The D values measured as a function of sol aging time (Figure 5b) showed no apparent trend with sol aging time. The D values from the SMT studies are ~ 100 -fold larger than those reported for spin-coated mesoporous silica films under drier conditions.^{6,21,33}

DISCUSSION

Quantitative Assessment of Mesopore Alignment and Order. The representative SMT results depicted in Figure 4 demonstrate that with the exception of sols aged to near the gelation time (~ 19 h), the majority of materials comprised well-ordered monodomains in which the average mesopore alignment was along the flow direction. These monodomains extended over distances of several millimeters. The high degree of pore alignment and order in the present materials stands in stark contrast to prior results from spin-coated mesoporous silica films, in which organized domains only a few tens to hundreds of micrometers in size were observed.^{6,34} These previous materials exhibited widely variable domain alignments, even when spin-coating methods meant to induce mesopore alignment along a particular direction were employed.⁶ Their “polycrystalline” nature clearly reflects the participation of nucleation and growth processes in domain formation.³⁴ The organized domains in the present samples were produced instead by flow alignment of hexagonally organized cylindrical mesophases already present in the sol.¹⁸ The materials organization was quantitatively assessed on the basis of two distinct parameters: (i) the average mesopore alignment relative to the expected direction and (ii) the materials order parameter, which reflects the distribution of mesopore orientations around the average alignment direction.

Quantitative assessment of the *average* mesopore alignment was accomplished by calculating the average in-plane trajectory angle, $\bar{\beta}$, for all individual trajectories acquired from three replicate samples at each aging time. Table 1 presents these results. For samples prepared from sols aged for ≤ 16 h, $\bar{\beta}$ was found to be 0° (the expected alignment) within the error of sample alignment on the microscope (i.e., $\pm 5^\circ$). In contrast, significant deviations from the flow direction were found for sols aged for 20 h, and $\bar{\beta}$ also varied widely between replicate samples. For the three replicate samples from which the 20 h data in Table 1 were obtained, the individual $\bar{\beta}$ values were 51° (data in Figure 4), 10° , and -2° . Comparison of the results obtained for samples aged for ≤ 16 h with those aged for 20 h demonstrates that effective flow alignment requires the injection of a fluid sol into the microfluidic channel. Although somewhat more variable, the SAXS results provide support for this conclusion. As shown in Table 1, the greatest deviations from 0° were again observed for the sol aged for 20 h, as demonstrated by the large error bar (95% confidence interval) on $\bar{\beta}$. The greater variability in the SAXS results may reflect

Table 1. SMT and SAXS Data Compiled from Series of Replicate Samples^a

aging time (h)	SMT				2D SAXS				
	n_1^b	$\bar{\beta}^c$	$\langle P \rangle$	$\langle \Delta\beta \rangle^d$	n_2^e	$\bar{\beta}^f$	$\langle P \rangle$	$\langle \Delta\beta \rangle^g$	d spacing (nm)
0	883	3 ± 1	0.88 ± 0.02	14	6	-16 ± 16	0.66 ± 0.13	24	5.30 ± 0.04
4	997	2 ± 1	0.86 ± 0.02	15	3	0 ± 1	0.81 ± 0.02	18	5.26 ± 0.03
8	1053	-3 ± 1	0.80 ± 0.03	18	6	-15 ± 20	0.75 ± 0.07	21	5.26 ± 0.06
12	1173	-2 ± 1	0.86 ± 0.02	15	3	10 ± 4	0.75 ± 0.20	20	5.26 ± 0.02
16	1038	3 ± 1	0.79 ± 0.02	19	3	-5 ± 6	0.77 ± 0.05	20	5.31 ± 0.02
20	886	25 ± 3	0.37 ± 0.04	34	3	-8 ± 100	0.39 ± 0.38	31	5.31 ± 0.01

^aError bars give the 95% confidence intervals of the mean values. ^bNumber of trajectories analyzed from three different samples at each aging time. ^cAverage trajectory orientation in degrees relative to the expected alignment direction, given as the arithmetic mean of all individual trajectory orientations. ^dAverage width of the trajectory angle distribution in degrees derived from the SMT data. ^eNumber of 2D SAXS measurements analyzed (three measurements were made per sample). ^fAverage alignment of the hexagonal mesopores in degrees relative to the expected alignment direction, determined from three to six replicate SAXS measurements. ^gAverage width of the hexagonal mesopore orientation distribution determined by SAXS (i.e., $\langle \Delta\beta \rangle$ is equal to σ in eq 3).

differences in the pore populations probed: SAXS measurements probe pore organization throughout the monolith, while TIRF-mode SMT probes only those pores within ~ 200 nm of the gel–glass interface.

Quantitative data on the mesopore order was obtained from the widths of the SMT trajectory angle distributions (Figure 4). The widths of the scattering peaks in the SAXS anisotropy data (Figure 2c) provided similar information. In both cases, the data obtained actually represent $f(\beta)$, a 2D projection of the 3D pore orientation distribution function.^{35,36} For materials with cylindrical symmetry, 3D order is most often reported as the average value of the second Legendre polynomial. However, as in previous reports,^{6,24} a 2D order parameter, $\langle P \rangle$, was employed here instead. $\langle P \rangle$ is defined as follows:

$$\langle P(\Delta\beta) \rangle = 2\langle \cos^2(\Delta\beta) \rangle - 1 \quad (1)$$

where $\Delta\beta = \beta - \bar{\beta}$, where the β values represent the individual trajectory angles. $\Delta\beta$ defines the deviation of each trajectory angle from the average value for a particular sample at each aging time. The value of $\langle \cos^2(\Delta\beta) \rangle$ is given by

$$\langle \cos^2(\Delta\beta) \rangle = \frac{\int_0^\pi f(\Delta\beta) \cos^2(\Delta\beta) d(\Delta\beta)}{\int_0^\pi f(\Delta\beta) d(\Delta\beta)} \quad (2)$$

In practice, $\langle \cos^2(\Delta\beta) \rangle$ was determined as the arithmetic mean of the $\cos^2(\Delta\beta)$ values from the single-molecule trajectories. $\langle P \rangle = 1.0$ for a perfectly aligned mesophase, while for a totally disordered population, $\langle P \rangle = 0.0$.

Several factors motivated the use of this alternative 2D order parameter. For the SMT data, the out-of-plane disorder is assumed to be much smaller than the in-plane disorder. The shear rate during channel filling is inversely proportional to the channel dimension, suggesting a narrower orientation distribution in the out-of-plane direction. The observation of aligned pores extending for tens of micrometers in the SMT data provided support for this assumption. Were the pores tilted out of the image plane by only a few degrees, they would appear much shorter than observed (see Figure 3), as they would extend beyond the excitation volume of the microscope. While the orientation distribution function was expected to be cylindrically symmetric for the SAXS samples, comparison with SMT data required the use of the same order parameter.

The $\langle P \rangle$ values obtained from SMT data demonstrate that highly ordered mesoporous materials can be obtained from sols aged for ≤ 16 h. As shown in Table 1, results derived from several thousand trajectories produced relatively constant $\langle P \rangle$ values ranging from 0.88 to 0.79. These values are similar to those reported previously for individual domains in spin-coated mesoporous silica films.⁶ A marked decrease in $\langle P \rangle$ was observed for samples prepared from sols aged for 20 h, for which $\langle P \rangle = 0.37$. This same trend in order with sol aging time was observed in three replicate sample series. The order parameters obtained from these individual series are plotted in Figure 6. The average width of the individual distributions provides a more fundamental view of materials order. These values are given in Table 1 as $\langle \Delta\beta \rangle$. Average distribution widths of $14\text{--}19^\circ$ were obtained for samples prepared well before sol gelation. An increase in the average distribution width to 34° occurred near the time of gelation.

The SAXS anisotropy data depict a similar level of mesopore orientational order and a similar trend with sol aging time. In this case, because of difficulties with background subtraction,

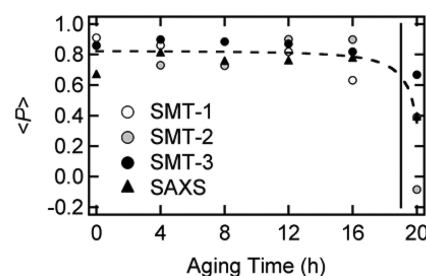


Figure 6. Order parameters, $\langle P \rangle$, measured for flow-aligned silica monoliths as a function of sol aging time prior to injection into the microfluidic channel. Shown are SMT data from three replicate sample series along with SAXS data. The data depict a constant, high level of organization up to approximately the gelation time (~ 19 h, vertical line), beyond which an abrupt decrease in order was observed. The dashed line has been included to highlight this trend.

the results were fit to Gaussian functions, and their widths, σ , were used to determine the associated $\langle P \rangle$ values:

$$\langle P \rangle \approx 2 \cos^2 \sigma - 1 \quad (3)$$

The values obtained are given in Table 1 and also are plotted along with the SMT results in Figure 6. The $\langle P \rangle$ values obtained by SAXS provide strong supporting evidence for the high level of materials order deduced from the SMT data. However, almost all of the SAXS $\langle P \rangle$ values are modestly smaller than those from the SMT data. These differences are easily attributable to differences in both fundamental and experimental aspects of the measurements. SAXS probes periodic structures in the monoliths, while SMT probes the alignment of individual mesopores that support 1D diffusion. Furthermore, SAXS probes the entire monolith thickness, while TIRF-mode SMT probes materials organization only near the gel–glass interface.

Mechanism for Organization of Flow-Aligned Mesopores. The SMT and SAXS results demonstrate that mesopore alignment and order is strongly dependent upon the sol aging time. Microfluidic channels filled well before gelation yield materials comprising large, well-ordered monodomains of mesopores aligned along the flow direction. In contrast, those filled close to the time of sol gelation yield monoliths in which the mesopores are misaligned and substantially more disordered. A simple model has been developed to explain these observations, as shown in Figure 7. Under the conditions employed, as-prepared (fresh) sols incorporate cylindrical surfactant micelles that are organized in randomly aligned domains. Prior to gelation, the surfactant mesophase is easily aligned by shear forces during filling of the microfluidic channels. The mesophase remains aligned during condensation of the silica precursors, which ultimately form a rigid gel around the micelles. Importantly, the sols remain sufficiently fluid until just before gelation, allowing for well-aligned materials to be prepared. However, for sols aged near or beyond the gelation time, the transition to a gel state occurs in the original vessel and locks in the original mesophase orientations within the sol. Injection of these rigid, polycrystalline materials into the microfluidic channel produces a monolith comprising misaligned, disordered mesopores. The mesopore order may reflect whatever alignment/order was originally present, or the mesophase may be broken up as it is infused into the microfluidic channel. The former mechanism is believed to be more important, as evidenced by the 20 h data shown in Figure

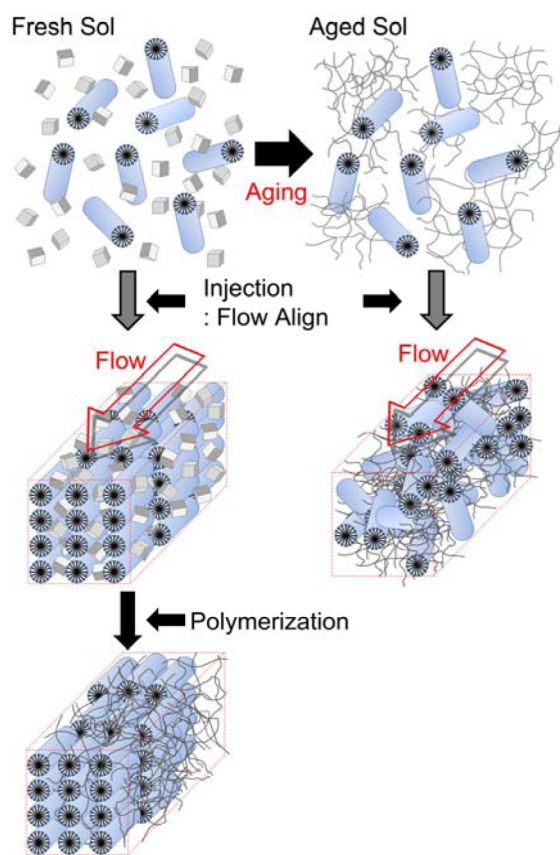


Figure 7. Model for the trend in mesopore order as a function of sol aging time. Surfactant-templated sols injected into microfluidic channels or capillaries prior to gelation are strongly aligned by shear flow during injection. Subsequent gelation of the sol forms a rigid matrix incorporating well-aligned mesopores. For sols close to the gelation time, the rigid gel structure has already begun to form around randomly aligned domains in the original vessel. These sols are not strongly aligned by flow during injection into the channels and capillaries and may be broken up by strong mechanical forces during injection.

4 and the associated replicate measurements. In these cases, the average mesopore alignment ($\bar{\beta}$) values fluctuate from sample to sample and can be far from the expected value of 0° . The 20 h SAXS data shown in Figure 2c depict a similar deviation from the expected $\bar{\beta}$ value of 0° for a similarly prepared sample. Taken together, these results suggest that “large” preformed domains present in the original vessel are loaded into the channel. These domains are not strongly aligned by the flow process when infused into the channel near the time of gelation. Were such domains broken up by infusion into the channel, small, randomly aligned domains similar to those observed for spin-coated films^{6,20} and exhibiting $\bar{\beta} = 0^\circ$ would be expected.

CONCLUSION

We have demonstrated that well-ordered mesoporous silica monoliths can be obtained by flow alignment of viscous, surfactant-templated sols within etched-glass microfluidic channels. The orientational alignment of open, surfactant-filled mesopores in these materials was assessed by tracking the motions of single molecules exhibiting 1D diffusion. Confirmation of materials alignment and order was obtained by SAXS anisotropy measurements. The mesopore organization was explored as a function of sol aging time. Microfluidic

channels filled well before gelation of the sol were shown to incorporate large mesoporous monodomains having average pore alignments within a few degrees of the expected direction over distances of several millimeters. These domains exhibited a high degree of mesopore orientational order, producing 2D order parameters averaging between 0.79 and 0.88. Channels filled near the time of sol gelation exhibited substantially greater variability in the average pore alignment and markedly reduced pore order, yielding order parameters near 0.35. The results of this study demonstrate that highly aligned, well-ordered mesoporous silica monoliths having applications in capillary- and/or microfluidic-based chemical separations can be obtained by simple flow alignment procedures. They also provide important guidance regarding the sample preparation conditions required in order to achieve optimum mesopore alignment: fresh sols or those aged for only brief periods of time should be employed.

ASSOCIATED CONTENT

Supporting Information

Structure of OPDI, additional polarization-dependent imaging data, MSD plots, and representative wide-field fluorescence videos (AVI). This material is available free of charge via the Internet at <http://pubs.acs.org>.

AUTHOR INFORMATION

Corresponding Author

*E-mail: ito@ksu.edu (T.I.) and higgins@ksu.edu (D.A.H.).

Notes

The authors declare no competing financial interest.

ACKNOWLEDGMENTS

The authors acknowledge support from the Division of Chemical Sciences, Geosciences, and Biosciences, Office of Basic Energy Sciences, U.S. Department of Energy (DE-SC0002362). Prof. Chris Culbertson is thanked for helpful suggestions on preparing microfluidic devices. SAXS measurements were carried out at the Characterization Facility at the University of Minnesota, which is supported by the NSF MRSEC Program. Linda Sauer and Michael Manno are thanked for their help with SAXS measurements.

REFERENCES

- (1) Beck, J. S.; Vartuli, J. C.; Roth, W. J.; Leonowicz, M. E.; Kresge, C. T.; Schmitt, K. D.; Chu, C. T.-W.; Olson, D. H.; Sheppard, E. W.; McCullen, S. B.; Higgins, J. B.; Schlenker, J. L. *J. Am. Chem. Soc.* **1992**, *114*, 10834–10843.
- (2) Kresge, C. T.; Leonowicz, M. E.; Roth, W. J.; Vartuli, J. C.; Beck, J. S. *Nature* **1992**, *359*, 710–712.
- (3) Selvam, P.; Bhatia, S. K.; Sonwane, C. G. *Ind. Eng. Chem. Res.* **2001**, *40*, 3237–3261.
- (4) Fan, J.; Boettcher, S. W.; Tsung, C.-K.; Shi, Q.; Schierhorn, M.; Stucky, G. D. *Chem. Mater.* **2008**, *20*, 909–921.
- (5) Innocenzi, P.; Malfatti, L.; Kidchob, T.; Falcaro, P. *Chem. Mater.* **2009**, *21*, 2555–2564.
- (6) Tran Ba, K. H.; Everett, T. A.; Ito, T.; Higgins, D. A. *Phys. Chem. Chem. Phys.* **2011**, *13*, 1827–1835.
- (7) Tolbert, S. H.; Firouzi, A.; Stucky, G. D.; Chmelka, B. F. *Science* **1997**, *278*, 264–268.
- (8) Walcarius, A.; Sibottier, E.; Etienne, M.; Ghanbaja, J. *Nat. Mater.* **2007**, *6*, 602–608.
- (9) Goux, A.; Etienne, M.; Aubert, E.; Lecomte, C.; Ghanbaja, J.; Walcarius, A. *Chem. Mater.* **2009**, *21*, 731–741.
- (10) Miyata, H. *Microporous Mesoporous Mater.* **2007**, *101*, 296–302.

- (11) Miyata, H.; Kuroda, K. *J. Am. Chem. Soc.* **1999**, *121*, 7618–7624.
- (12) Wu, C.-W.; Ohsuna, T.; Edura, T.; Kuroda, K. *Angew. Chem., Int. Ed.* **2007**, *46*, 5364–5368.
- (13) Yamaguchi, A.; Kaneda, H.; Fu, W.; Teramae, N. *Adv. Mater.* **2008**, *20*, 1034–1037.
- (14) Yamaguchi, A.; Teramae, N. *Anal. Sci.* **2008**, *24*, 25–30.
- (15) Melosh, N. A.; Davidson, P.; Feng, P.; Pine, D. J.; Chmelka, B. F. *J. Am. Chem. Soc.* **2001**, *123*, 1240–1241.
- (16) Trau, M.; Yao, N.; Kim, E.; Xia, Y.; Whitesides, G. M.; Aksay, I. A. *Nature* **1997**, *390*, 674–676.
- (17) Rühle, B.; Davies, M.; Lebold, T.; Bräuchle, C.; Bein, T. *ACS Nano* **2012**, *6*, 1948–1960.
- (18) Göltner, C. G.; Antonietti, M. *Adv. Mater.* **1997**, *9*, 431–436.
- (19) Jung, C.; Kirstein, J.; Platschek, B.; Bein, T.; Budde, M.; Frank, I.; Müllen, K.; Michaelis, J.; Bräuchle, C. *J. Am. Chem. Soc.* **2008**, *130*, 1638–1648.
- (20) Kirstein, J.; Platschek, B.; Jung, C.; Brown, R.; Bein, T.; Bräuchle, C. *Nat. Mater.* **2007**, *6*, 303–310.
- (21) Zürner, A.; Kirstein, J.; Döblinger, M.; Bräuchle, C.; Bein, T. *Nature* **2007**, *450*, 705–709.
- (22) Ito, S.; Fukuya, S.; Kusumi, T.; Ishibashi, Y.; Miyasaka, H.; Goto, Y.; Ikai, M.; Tani, T.; Inagaki, S. *J. Phys. Chem. C* **2009**, *113*, 11884–11891.
- (23) Moerner, W. E.; Fromm, D. P. *Rev. Sci. Instrum.* **2003**, *74*, 3597–3619.
- (24) Kirkeminde, A. W.; Torres, T.; Ito, T.; Higgins, D. A. *J. Phys. Chem. B* **2011**, *115*, 12736–12743.
- (25) Liao, Y.; Yang, S. K.; Koh, K.; Matzger, A. J.; Biteen, J. S. *Nano Lett.* **2012**, *12*, 3080–3085.
- (26) Tran-Ba, K.-H.; Finley, J. J.; Higgins, D. A.; Ito, T. *J. Phys. Chem. Lett.* **2012**, *3*, 1968–1973.
- (27) Doshi, D. A.; Gibaud, A.; Goletto, V.; Lu, M.; Gerung, H.; Ocko, B.; Han, S. M.; Brinker, C. J. *J. Am. Chem. Soc.* **2003**, *125*, 11646–11655.
- (28) Meyer, A. R.; Clark, A. M.; Culbertson, C. T. *Lab Chip* **2006**, *6*, 1355–1361.
- (29) Fu, Y.; Ye, F.; Sanders, W. G.; Collinson, M. M.; Higgins, D. A. *J. Phys. Chem. B* **2006**, *110*, 9164–9170.
- (30) Levy, G. Particle Tracker. <http://rsb.info.nih.gov/ij/>, 2009.
- (31) Dunn, G. *Statistical Evaluation of Measurement Errors: Design and Analysis of Reliability Studies*; Arnold: London, 2004.
- (32) Schmidt, T.; Schütz, G. J.; Baumgartner, W.; Gruber, H. J.; Schindler, H. *Proc. Natl. Acad. Sci. U.S.A.* **1996**, *93*, 2926–2929.
- (33) Ye, F.; Higgins, D. A.; Collinson, M. M. *J. Phys. Chem. C* **2007**, *111*, 6772–6780.
- (34) Jung, C.; Schwaderer, P.; Dethlefsen, M.; Köhn, R.; Michaelis, J.; Bräuchle, C. *Nat. Nanotechnol.* **2011**, *6*, 87–92.
- (35) Ehlich, D.; Takenaka, M.; Okamoto, S.; Hashimoto, T. *Macromolecules* **1993**, *26*, 189–197.
- (36) Jain, A.; Hall, L. M.; Garcia, C. B. W.; Gruner, S. M.; Wiesner, U. *Macromolecules* **2005**, *38*, 10095–10100.